OPEN ACCESS
CellPress

Cell Reports
Article

Ergothioneine Maintains Redox and Bioenergetic Homeostasis Essential for Drug Susceptibility and Virulence of *Mycobacterium tuberculosis*

Vikram Saini,[1,2,7] Bridgette M. Cumming,[5,7] Loni Guidry,[1] Dirk A. Lamprecht,[5] John H. Adamson,[5] Vineel P. Reddy,[1] Krishna C. Chinta,[1] James H. Mazorodze,[5] Joel N. Glasgow,[1] Melissa Richard-Greenblatt,[3] Anaximandro Gomez-Velasco,[3] Horacio Bach,[3] Yossef Av-Gay,[3] Hyungjin Eoh,[4] Kyu Rhee,[4] and Adrie J.C. Steyn[1,2,5,6,*]
[1]Department of Microbiology, University of Alabama at Birmingham, Birmingham, AL 35294, USA
[2]Centers for AIDS Research and Free Radical Biology, University of Alabama at Birmingham, Birmingham, AL 35294, USA
[3]Department of Medicine, University of British Columbia, Vancouver, BC V6H 3Z6, Canada
[4]Department of Medicine, Weill Cornell Medical College, New York, NY 10065, USA
[5]KwaZulu-Natal Research Institute for Tuberculosis and HIV, Durban 4001, South Africa
[6]Department of Pathology, Nelson Mandela School of Medicine, University of KwaZulu-Natal, Durban 4001, South Africa
[7]Co-first author
*Correspondence: asteyn@uab.edu
http://dx.doi.org/10.1016/j.celrep.2015.12.056

SUMMARY

The mechanisms by which *Mycobacterium tuberculosis* (*Mtb*) maintains metabolic equilibrium to survive during infection and upon exposure to antimycobacterial drugs are poorly characterized. Ergothioneine (EGT) and mycothiol (MSH) are the major redox buffers present in *Mtb*, but the contribution of EGT to *Mtb* redox homeostasis and virulence remains unknown. We report that *Mtb* WhiB3, a 4Fe-4S redox sensor protein, regulates EGT production and maintains bioenergetic homeostasis. We show that central carbon metabolism and lipid precursors regulate EGT production and that EGT modulates drug sensitivity. Notably, EGT and MSH are both essential for redox and bioenergetic homeostasis. Transcriptomic analyses of EGT and MSH mutants indicate overlapping but distinct functions of EGT and MSH. Last, we show that EGT is critical for *Mtb* survival in both macrophages and mice. This study has uncovered a dynamic balance between *Mtb* redox and bioenergetic homeostasis, which critically influences *Mtb* drug susceptibility and pathogenicity.

INTRODUCTION

Tuberculosis (TB) is the second most common cause of death from an infectious agent after HIV. This is largely due to the ability of *Mycobacterium tuberculosis* (*Mtb*) to remain in a dormant, drug-tolerant state for decades in humans before emerging to cause active disease in ~10% of those infected. *Mtb* is exposed to environments with a wide range of available carbon sources, reactive oxygen intermediates (ROIs), and reactive nitrogen intermediates (RNIs) inside the host that may cause cell death. Therefore, it is strongly anticipated that the ability of *Mtb* to maintain redox balance and metabolic homeostasis is critical to its pathogenicity and virulence (Kumar et al., 2011). In addition, some front-line TB drugs such as isoniazid are prodrugs that require bioreduction by *Mtb* for anti-mycobacterial activity (Lei et al., 2000). Thus, a fundamental challenge to global TB control is to understand the mechanisms by which *Mtb* adapts to diverse carbon sources and redox environments encountered in the host.

Mtb produces mycothiol (MSH; Figure 1A), which acts as a major redox couple to protect against various redox stressors and anti-TB drugs (Buchmeier et al., 2003; Rawat et al., 2007). *Mtb* also produces a second thiol couple, ergothioneine (EGT; Figure 1B), a sulfur-containing histidine derivative with potent antioxidant properties (Genghof, 1970; Hand and Honek, 2005). However, despite considerable effort, roles for EGT in *Mtb* and its potential involvement in redox homeostasis and pathogenesis remain unknown. Recently, we have shown that EGT levels in *Mtb* are modulated by protein phosphorylation during transition into late states of growth (Richard-Greenblatt et al., 2015), yet it is still unclear why mycobacteria produce both EGT and MSH to maintain redox homeostasis.

Redox balance is essential for energy metabolism, including glycolysis, the tricarboxylic acid (TCA) cycle, and oxidative phosphorylation (OXPHOS). Despite this strong interdependence between redox homeostasis and energy metabolism, very few tools are available to investigate mycobacterial bioenergetics in real time and in a noninvasive manner. Since cellular respiration involves a complex interplay of biological factors, including the availability, nature, and concentration of oxidizable substrates as well as energy demand, methods for detecting such bioenergetic perturbations in *Mtb* will be of great value.

We previously demonstrated that WhiB3, an *Mtb* 4Fe-4S cluster redox sensor and virulence protein, maintains intracellular redox homeostasis of the mycobacterial cell to provide metabolic and cellular integrity (Singh et al., 2007, 2009; Steyn et al., 2002). In this study, we examined how WhiB3 controls

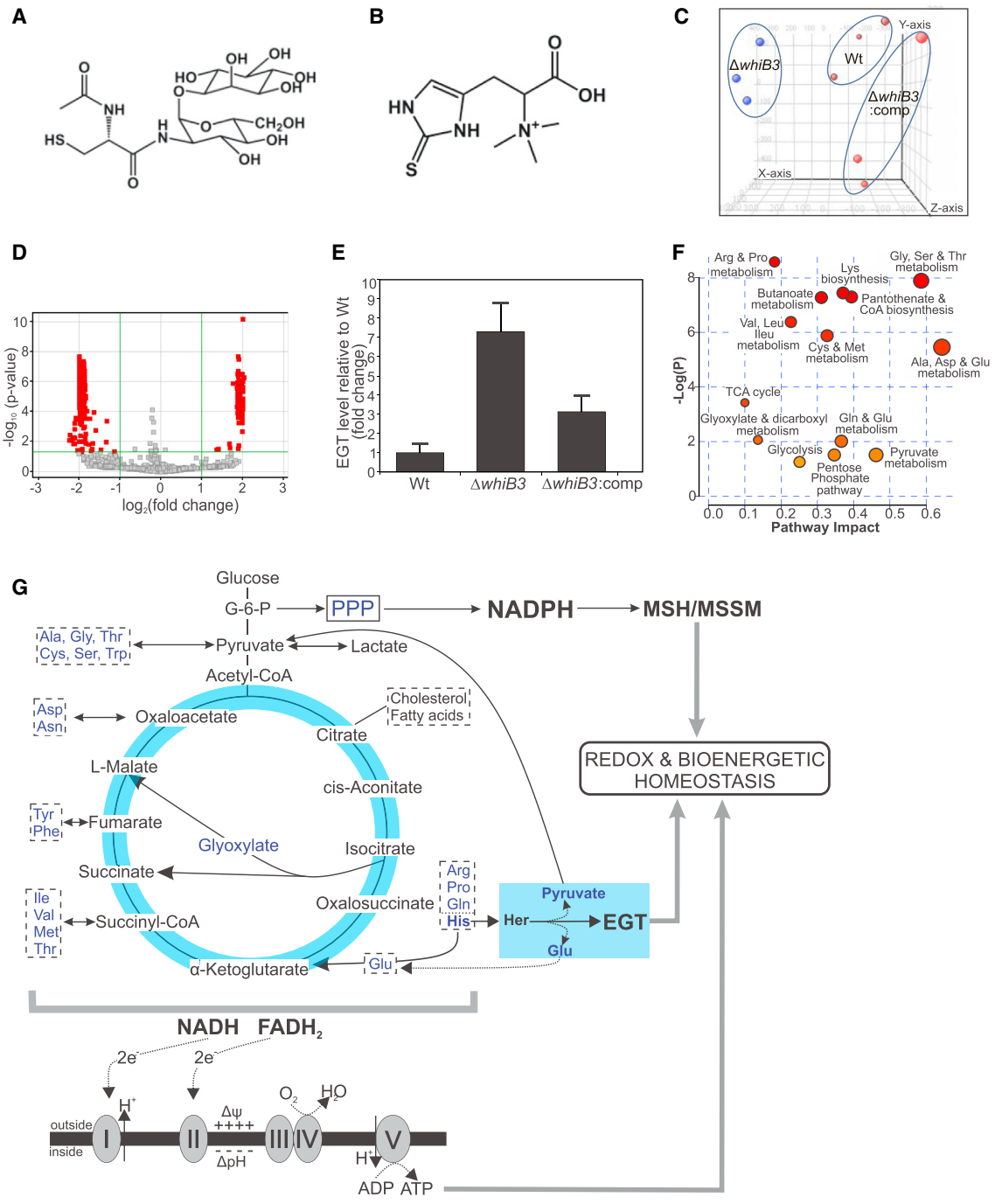

Figure 1. Metabolomic Analysis of Δ*whiB3* Demonstrates Increased Levels of EGT

(A and B) Chemical structures of (A) MSH and (B) EGT.

(C) Principal-component analysis shows that WT *Mtb*, Δ*whiB3*, and Δ*whiB3*:comp strains can be distinguished based on their overall metabolomic profiles. For metabolomic analysis, each strain was independently examined at least twice in triplicate.

(D) Volcano plot of metabolites in WT *Mtb* and Δ*whiB3* plotted as fold change versus significance. The green lines demarcate metabolites with a greater than 2-fold change on the x axis and a corrected p value < 0.05 (289/3,327 molecules). Metabolites with less than a 2-fold change and/or $p > 0.05$ are shown in gray. See also Table 1.

(E) Independent validation of EGT production in WT *Mtb*, Δ*whiB3*, and Δ*whiB3*:comp based on LC-MS analysis after growth on medium containing 5 mM acetate. Error bars denote SEM.

(F) Untargeted metabolite profiling assessed by MetPa enrichment analysis, based on changes in the relative abundance of metabolites (see also Figure S1 and Table S1), indicate that WhiB3 has a profound effect on *Mtb* metabolism, especially carbon catabolism, bioenergetic metabolism, amino acid metabolism, the pentose phosphate pathway (PPP), and glycolysis.

(legend continued on next page)

redox and bioenergetic homeostasis in *Mtb* to moderate virulence. We used a combination of metabolomic, bioenergetic, and transcriptomic approaches and established links between WhiB3 and bioenergetic homeostasis and EGT, a major redox buffer. We characterized the genetic architecture of the EGT biosynthesis operon in *Mtb* and assessed the contribution of EGT in protection against oxidative stress, in antimycobacterial drug susceptibility, and in bioenergetic homeostasis. Further, we examined a link between *Mtb* central carbon catabolism and EGT production and the relationship between EGT and MSH biosynthesis. Using genome-wide expression analysis of genetically defined mutants of MSH and EGT biosynthesis, we identified differentially regulated genes common to all *Mtb* mutants. Finally, using macrophages and a mouse model of infection, we establish that maintaining redox balance and bioenergetic homeostasis is essential for *Mtb* virulence.

RESULTS

WhiB3 Regulates EGT Production in *Mtb*

Since *Mtb* WhiB3 is an intracellular redox sensor (Singh et al., 2009), we sought to identify redox-responsive metabolites regulated by WhiB3. We analyzed the metabolomes of *Mtb* (H37Rv), Δ*whiB3* and the corresponding *whiB3*-complemented strain (Δ*whiB3*:comp), under rigorously controlled conditions (de Carvalho et al., 2010). Metabolites were separated by high-performance liquid chromatography (HPLC) and detected by electrospray ionization coupled to mass time-of-flight mass spectrometry (liquid chromatography-tandem mass spectrometry [LC-MS/MS]) as previously described (Rhee et al., 2011). Among the statistically significant differences detected (Figures 1C, 1D, and S1) was the increased production of EGT in Δ*whiB3*. Independent validation showed a 7.3-fold increase in EGT levels in Δ*whiB3* (Figure 1E), and complementation of *whiB3* restored the EGT content to near wild-type levels (Figure 1E).

Next, we performed Metabolic Pathway Analysis (MetPa), which combines pathway enrichment analysis with pathway topology, to detect metabolic differences between *Mtb* and Δ*whiB3* (Everts et al., 2014; Nandakumar et al., 2014). This analysis highlighted changes in the abundance of metabolites of biochemical pathways in Δ*whiB3*, including glycolysis, the pentose phosphate pathway, the TCA cycle, and several amino acid biosynthesis pathways (Figure 1F; Tables 1 and S1). The pyruvate node is of particular significance as it is a key intermediate of many amino acid metabolism pathways, glycolysis, and the TCA cycle (Figure 1G; Table S1).

Overall, these metabolomic data demonstrate that WhiB3 modulates the production of EGT. Further analyses revealed that WhiB3 also modulates the production of several amino acids, which act as anaplerotic and cataplerotic substrates and converge on glycolysis and the TCA cycle to affect energy metabolism (Figure 1G).

Table 1. MetPa Analysis of Pathways Altered in Δ*whiB3* Compared to WT *Mtb*

	Metabolites			
KEGG Pathway Name	Total	Hits	p Value	Impact
Arginine and proline metabolism	41	12	0.000189	0.19
Glycine, serine, and threonine metabolism	32	10	0.000378	0.60
Lysine biosynthesis	13	6	0.000588	0.38
Pantothenate and CoA biosynthesis	23	8	0.000681	0.41
Butanoate metabolism	18	7	0.000699	0.32
Valine, leucine, and isoleucine biosynthesis	26	8	0.00171	0.24
Cysteine and methionine metabolism	34	9	0.00282	0.34
Alanine, aspartate, and glutamine metabolism	18	6	0.0043	0.66
Citrate cycle (TCA cycle)	20	5	0.0327	0.11

Metabolic Pathway Analysis (MetPa) combines pathway enrichment analysis with pathway topology analysis to identify the most relevant pathways under the specified conditions. MetPa uses the KEGG metabolic pathways as the backend knowledge base and integrates univariate analysis, over-representation analysis, Global Test, GlobalAncova, and network topology analysis into pathway analysis. The total/maximum importance of each pathway = 1; pathway impact value = cumulative % from the matched metabolic nodes. Pathways with the most significant change ($p \leq 0.05$) are listed. KEGG, Kyoto Encyclopedia of Genes and Genomes; TCA, tricarboxylic acid. See also Table S1.

WhiB3 Maintains Bioenergetic Homeostasis in *Mtb*

Next, we optimized extracellular flux analysis previously applied only to eukaryotic cells, for the study of *Mtb*. In this method, fluorescence sensors measure dissolved extracellular oxygen and proton concentration in real time in a microtransient chamber formed when the probes are in the measurement position. Inhibitors, modulators, or substrates can be added during the run through delivery ports in the cartridge. This technology allowed us to accurately measure the oxygen consumption rate (OCR) and the extracellular acidification rate (ECAR) of *Mtb* cells in real time in a noninvasive manner (Figure 2A). The OCR and ECAR are direct and highly sensitive measures of cellular metabolic activity (Ferrick et al., 2008). ECAR gives a measure of H^+ extrusion associated with carbon catabolism via glycolysis and the TCA cycle, whereas OCR is indicative of cellular respiration due to OXPHOS. The cell energy phenotype can be deduced from a phenogram (plotting of OCR versus ECAR) that illustrates metabolic shifts between substrate oxidation and glycolysis. We used pyruvate, identified as a key glycolytic intermediate (Figure 1G; Table S1), as the sole carbon source in extracellular flux analyzer (XF) bioenergetic assays. We used carbonyl cyanide m-chlorophenylhydrazone (CCCP), a membrane uncoupler, to examine the capacity of WhiB3 to maintain bioenergetic

(G) EGT is linked to the metabolism of histidine (His) as it is derived from hercynine (Her), and MSH biosynthesis is regulated by NADPH produced by the PPP. Glycolysis and the TCA cycle both feed into the electron transport chain to regulate the electrical ($\Delta\psi$) and concentration (ΔpH) gradients across the membrane, which maintain bioenergetic homeostasis. Amino acids acting as anaplerotic and cataplerotic substrates are boxed.
See also Figure S1 and Table S1.

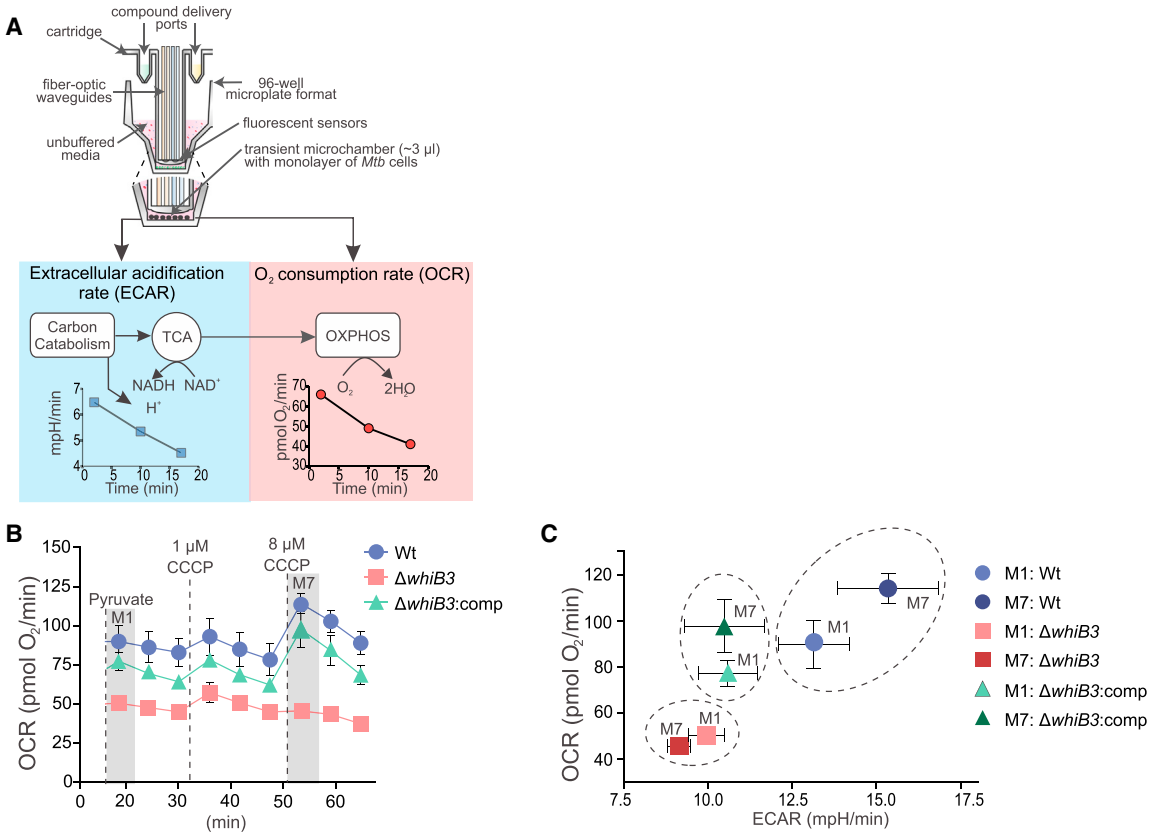

Figure 2. Extracellular Flux Analysis Demonstrates the Bioenergetic Deficiency of Δ*whiB3*

(A) Diagram of the probe of an XF96 cartridge and a well of the cell culture microplate. During the assay, ECAR is measured as an indication of H^+ production from carbon catabolism and OCR as an indication of OXPHOS.

(B) OCR profiles of WT *Mtb* H37Rv (blue), Δ*whiB3* (red), and Δ*whiB3*:comp (green) in the presence of pyruvate (50 µM, M1) and after addition of two aliquots of CCCP to a final concentration of 1 µM and 8 µM (M7) indicated by the vertical dotted lines.

(C) Phenogram of all three strains at M1 (after pyruvate addition) and M7 (after the second CCCP addition) demonstrating increased OCR and ECAR of WT *Mtb* H37Rv and Δ*whiB3*:comp after CCCP addition in contrast to the inability of Δ*whiB3* to respond to the uncoupling stress.

homeostasis upon uncoupling of OXPHOS from ATP production. In the presence of pyruvate, Δ*whiB3* had a significantly lower OCR than WT and Δ*whiB3*:comp (Figure 2B). After addition of CCCP (8 µM; M7), both the WT and Δ*whiB3*:comp strains responded to the uncoupling stress by increasing OCR (Figure 2B). The OCR and ECAR data from these experiments were plotted to generate a phenogram, which provides a visualization of the overall metabolic profiles of the different strains (Figure 2C). Our data show that Δ*whiB3*, in contrast to WT *Mtb*, did not respond with an increase in OCR or ECAR to re-establish membrane potential (M7, Figure 2C), indicating that Δ*whiB3* is bioenergetically deficient.

In sum, we optimized extracellular flux analysis for the study of *Mtb* bioenergetics. Adapting this technology toward *Mtb* has broad implications for studying bioenergetics of microbial pathogens in general. The results demonstrate that in the absence of WhiB3, *Mtb* cannot respire efficiently when the glycolytic intermediate pyruvate is the sole carbon source. This suggests that the absence of WhiB3 leads to dysfunctional respiration and confirms its involvement in maintaining bioenergetic homeostasis.

EGT Detection Using TLC

The study of EGT biosynthesis in bacteria has been hampered by the fact that EGT quenches the fluorescence of bimane derivatives, thereby making routine detection of EGT by HPLC analysis difficult. We therefore developed a rapid thin-layer chromatography (TLC)-based radioactive labeling assay and showed that pure EGT has an R_f value of ~0.46 (Figure S2A). TLC analysis of concentrated *M. smegmatis* (*Msm*) and *Mtb* extracts revealed bands with R_f values consistent with that of pure EGT (Figures 3A and S2A). LC-MS/MS analysis of these bands and an EGT standard revealed virtually identical retention times and confirmed them to be EGT (Figures 3B, 3C, and S2B). An earlier study in *Claviceps purpurea* showed that [2-^{14}C]-acetate could be used to label EGT (Heath and Wildy, 1956). However, we could not detect labeled EGT after TLC analysis of extracts from *Msm* cultured in the presence of [2-^{14}C]-acetate even though UV exposure revealed a band at the same position as pure EGT, indicating that EGT was present (Figure 3D). However, by using [^{35}S]-Cys as a precursor, we observed a labeled spot after TLC analysis with the same R_f value as the EGT identified by LC-MS/MS analysis (Figure 3E).

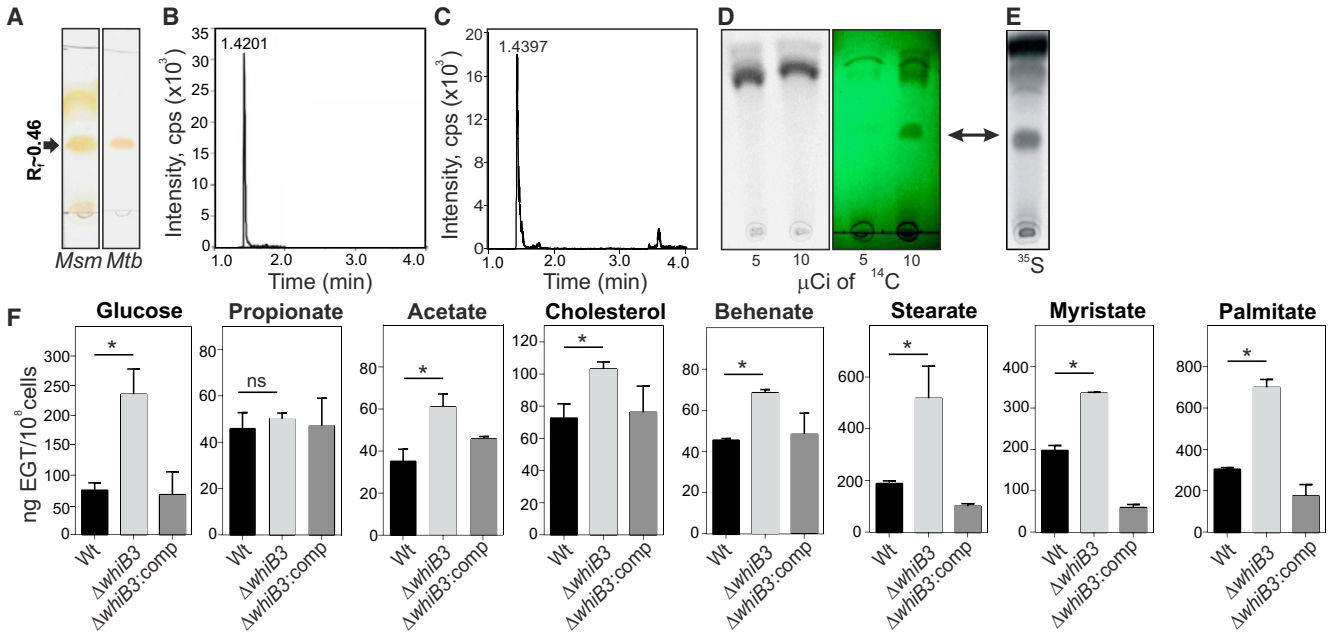

Figure 3. Detection of EGT by TLC Analysis and WhiB3 Regulation of EGT in Response to Carbon Catabolism

(A) TLC analysis of *Mtb* and *M. smegmatis* (*Msm*) extracts followed by application of 0.2% ethanolic Gibb's reagent. EGT appears as a brick-red spot with R_f values near 0.46.

(B) This band on the TLC plate was extracted and analyzed by LC-MS/MRM to confirm its identity as EGT. The main elution peak at a retention time of 1.4201 min represents EGT.

(C) LC-MS/MRM analysis of an EGT standard with a retention time of 1.4397 min confirmed the band in (B) is EGT.

(D) *Mtb* cells were grown in the presence of 5 or 10 μCi of [2-^{14}C]-acetate followed by extraction in water and TLC analysis using 50,000 counts. Exposure of the TLC plate to a phosphor storage screen and viewing by phosphoimaging (left) or a UV lamp at 256 nm revealed the EGT band (green image; EGT bands; arrow).

(E) EGT was detected in extracts of ^{35}S-cysteine-fed cultures followed by TLC and autoradiography and was confirmed by LC-MS/MS.

(F) LC-MS/MS quantitation of EGT in *Mtb*, Δ*whiB3*, and Δ*whiB3*:comp strains that were cultured in glucose, various fatty acids, or the breakdown products of β-oxidation as the sole carbon sources. Error bars represent SEM, n = 3, and *$p < 0.05$.

See also Figure S2.

Altogether, we have developed a simple radioactive TLC-based assay that facilitates the rapid, routine examination of EGT in mycobacteria and potentially other EGT-producing bacteria. Further, this method revealed differences in the biosynthetic pathways of either EGT or EGT precursors between fungi and mycobacteria.

WhiB3-Mediated Regulation of EGT Production Is Dependent on Central Carbon Metabolism

Since WhiB3 initiates the metabolic switchover to the preferred in vivo carbon source (fatty acids) and integrates redox signals with core intermediary metabolism (Singh et al., 2007, 2009), we sought to establish whether the type of carbon source influences WhiB3-mediated regulation of EGT production. LC-MS/MS was used to quantify intracellular EGT in *Mtb*, Δ*whiB3*, and Δ*whiB3*:comp grown in physiologically relevant concentrations (50 μM [Lee et al., 2013]) of carbon sources, including glucose, lipids, and lipid precursors. As shown in Figure 3F, Δ*whiB3* had significantly increased levels of EGT compared to WT or Δ*whiB3*:comp when grown in glucose, acetate, cholesterol, behenate, stearate, myristate, or palmitate and no difference when grown in propionate. EGT levels in WT *Mtb* ranged from 40 to over 300 ng/10^8 cells with higher (>200 ng/10^8 cells) levels occurring in cells grown in myristate (C-14), palmitate (C-16), and stearate (C-18). Δ*whiB3* grown in the same C-14, C-16, and C-18 fatty acids produced even higher levels of EGT (≥400 ng/10^8 cells). We observed EGT levels < 120 ng/10^8 cells in WT *Mtb* grown on glucose, propionate (C-3), acetate (C-2), behenate (C-22), and cholesterol (C-27). Δ*whiB3* grown in these substrates had similarly lower EGT levels albeit significantly higher than the WT, with the exception of glucose, where levels were > 250 ng EGT/10^8 cells. In sum, these data demonstrate that WhiB3 regulates EGT production in response to catabolism of a diverse set of fatty acid precursors and cholesterol.

The *Mtb* EGT Operon

In vitro reconstitution studies using protein preparations of *Erwinia tasmaniensis* and *Msm* (Seebeck, 2010), as well as a recent genetic study in *Msm* (Sao Emani et al., 2013), have provided biochemical and genetic evidence for EGT production in *Msm*. Analysis of the *Mtb* genome led us to predict that locus Rv3704c–Rv3700c constitutes the EGT biosynthetic operon. Figure 4C shows the genetic organization and biochemical pathway involved in EGT production and the link between EGT and MSH biosynthesis in *Mtb*. Examination of EGT production in *Mtb* CDC1551 and corresponding transposon mutants that disrupt *egtA* or *egtD* (hereafter referred to as *egtA*:Tn and *egtD*:Tn) revealed that *Mtb egtA*:Tn and *egtD*:Tn do not produce

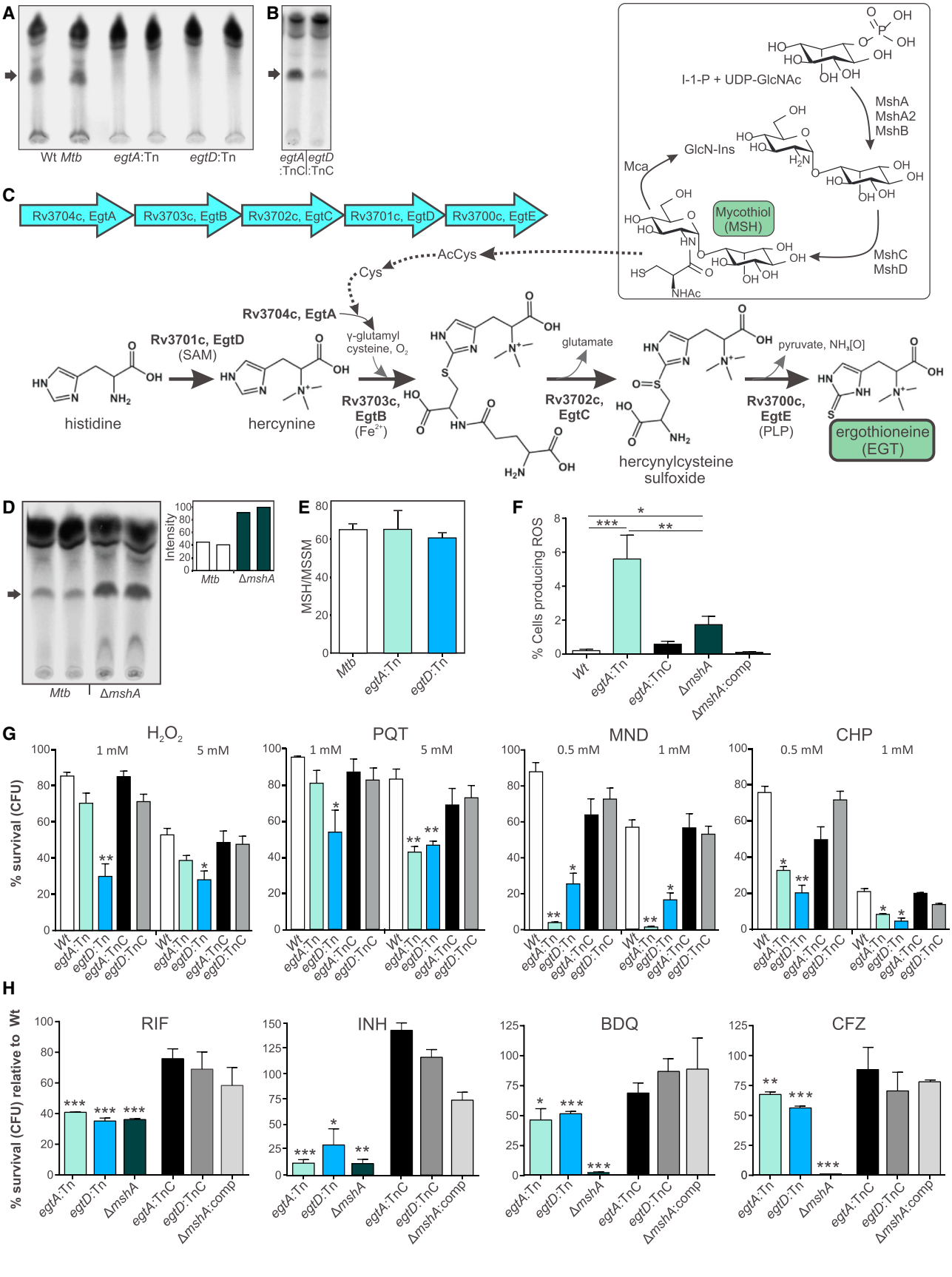

(legend on next page)

EGT (Figure 4A). Production of EGT in *egtA*:Tn was successfully complemented with the addition of the complete *egt* gene cluster (Rv3704c–Rv3700c, *egtA*:TnC) and partially complemented in *egtD*:Tn with the addition of *egtD* (*egtD*:TnC; Figure 4B). The arrangement of the *egt* genes, with *egtA*/*egtB* and *egtC*/*egtD* having overlapping stop and start codons (5′-GTGA-3′ and 5′-ATGA -3′, respectively), suggested that they may be operonic. RT-PCR analysis established that *egtA* through *egtD* are indeed operonic, while *egtE* is not (Figure S3). In sum, we have confirmed the genetic components and operonic organization (Rv3704c–Rv3700c) responsible for EGT biosynthesis in *Mtb*.

EGT and Mycobacterial Redox Balance

Next, to examine the biological significance of EGT, and whether EGT and MSH are linked metabolically, we measured EGT levels in *Mtb* defective in MSH production. We noticed substantially increased EGT levels in Δ*mshA* compared to WT (Figure 4D). HPLC analyses of reduced MSH (2MSH) and oxidized (disulfide) MSH (MSSM) levels in *Mtb* CDC1551, *egtA*:Tn, and *egtD*:Tn indicated that the MSH/MSSM ratio does not differ in the *Mtb* EGT mutants (Figure 4E).

We then examined the endogenous reactive oxygen species (ROS) levels in *Mtb* strains defective in EGT or MSH production. Flow cytometry analysis of WT, *egtA*:Tn, and Δ*mshA* following exposure to the ROS-responsive dye CellROX Green revealed that *egtA* and *mshA* mutants have a significantly increased percentage of cells that produce ROS under normal growth conditions (Figure 4F). Compared to WT, *egtA*:Tn had 25-fold and Δ*mshA* had 8-fold more ROS-producing cells. Further, the *egtA*:Tn strain had 3-fold more ROS-producing cells compared to Δ*mshA*. The increased EGT levels observed in Δ*mshA* (Figure 4D) likely mitigate the endogenous ROS in this mutant. We conclude that while a lack of MSH substantially increases levels of EGT, loss of EGT does not lead to a corresponding increase in MSH/MSSM, which may be the cause of increased endogenous ROS levels observed in the *egtA* mutant. These data establish a physiological link between MSH and EGT production in *Mtb* and confirm their role in controlling endogenous ROS.

Role of EGT in Protection against Oxidative Stress

The role of MSH in protecting mycobacteria from oxidative stress is well documented (Buchmeier et al., 2003; Miller et al., 2007). However, we know little about the role of EGT in combating oxidative stress in *Mtb*. We investigated the ability of EGT to protect *Mtb* under various conditions of oxidative stress. We observed that both *egtA*:Tn and *egtD*:Tn were significantly more sensitive than WT upon exposure to hydrogen peroxide (H_2O_2), paraquat (PQT), menadione (MND), and cumene hydroperoxide (CHP) (Figure 4G). Survival of *egtA*:Tn and *egtD*:Tn was reduced most significantly by CHP and MND. Compared to *egtA*:Tn, viability of *egtD*:Tn was significantly decreased following exposure to H_2O_2 or PQT (Figure 4G). We noted that *egtA*:Tn is susceptible only at the higher concentration of PQT. Complementation of the mutants restored protection against the oxidants, and viability was similar to that of WT *Mtb*. Altogether, these findings provide evidence that EGT protects *Mtb* from a diverse set of oxidative stressors.

EGT and Antimycobacterial Drug Susceptibility

The redox status and metabolic state of *Mtb* can affect its sensitivity to anti-TB drugs (Baek et al., 2011; Kumar et al., 2011; Nandakumar et al., 2014). Here, we tested the hypothesis that lack of EGT in *Mtb* modulates susceptibility to front-line anti-TB drugs. To address this, we used a colony-forming unit (CFU)-based viability assay to determine drug susceptibilities. We observed that, compared to WT *Mtb*, the minimal inhibitory concentration (MIC) of rifampicin (RIF), isoniazid (INH), bedaquiline (BDQ), and clofazimine (CFZ) was significantly reduced for the *egtA*:Tn, *egtD*:Tn, and Δ*mshA* strains (Table S2). At MIC values obtained for WT *Mtb*, the percentage survival of *egtA*:Tn, *egtD*:Tn, and Δ*mshA* was < 40% and < 25% of WT *Mtb* in the presence of RIF and INH, respectively (Figure 4H). Similarly, against CFZ and the recently developed drug BDQ, survival of *egtA*:Tn and *egtD*:Tn strains was reduced to < 70% and < 50% of WT *Mtb*, respectively. Genetic complementation of the *egtA*/*egtD* and *mshA* mutants reduced drug susceptibility to near wild-type levels. As shown in Figure 4H, drug susceptibilities of the *egt* mutants against INH and RIF were comparable to that of Δ*mshA* (MIC = 0.015 and 0.006 μg/ml, respectively). Of note, Δ*mshA* was significantly more susceptible to BDQ and CFZ compared to WT *Mtb* and the *egtA*/*D* mutants, revealing a greater role for MSH in protecting against these drugs. These data demonstrate that the lack of EGT results in increased susceptibility to anti-TB drugs and indicate that EGT and MSH are not fully redundant and have overlapping but distinct functional roles in *Mtb* physiology.

Figure 4. Genetic Characterization of the EGT Biosynthetic Operon in *Mtb*

(A) TLC and autoradiographic analyses of ^{35}S-cysteine-fed *egtA*:Tn, *egtD*:Tn, and the corresponding WT strain (*Mtb* CDC1551) indicate that disruption of *egtA* or *egtD* abrogates EGT production.

(B) Genetically complemented strains *egtA*:TnC and *egtD*:TnC produce EGT. Complementation in *egtD*:TnC appeared to be partial.

(C) Model depicts a putative link between the MSH and EGT pathways via Acetyl-Cys and Cys (indicated by dotted arrows).

(D) TLC and autoradiographic analyses of ^{35}S-cysteine-fed *Mtb* CDC1551 and its corresponding Δ*mshA* strain (duplicate samples) show increased EGT production in the mutant lacking MSH.

(E) HPLC measurement of reduced (MSH) and oxidized (MSSM) mycothiol. MSH/MSSM ratio is presented as the mean ± SD of three independent cultures.

(F) Flow-cytometric measurement of endogenous ROS with CellROX Green dye in *Mtb* revealed that the *egtA*:Tn and Δ*mshA* mutant had significantly more ROS-producing cells relative to WT (***$p < 0.001$, **$p < 0.005$, and *$p < 0.05$, respectively) or corresponding complemented strains.

(G) EGT protects *Mtb* against oxidative stress. Following exposure to H_2O_2, PQT, MND, and CHP, cells were plated and CFUs enumerated. Percentage survival was determined relative to untreated (UT) cells for each strain. Each column represents the mean ± SD ($n = 4$, *$p < 0.05$, and **$p < 0.01$) compared to the WT strain.

(H) Lack of EGT increases susceptibility of *Mtb* to RIF, INH, BDQ, and CFZ. Graphs show, at MIC values obtained for WT *Mtb*, the percentage survival (CFUs) of *egtA*:Tn, *egtD*:Tn, and Δ*mshA* relative to the WT strain (see also Table S2). Complementation restored drug sensitivities to near WT levels. Each column represents the mean ± SD ($n = 4$, *$p < 0.05$, **$p < 0.01$, and ***$p < 0.001$) compared to WT strain.

See also Figure S3 and Table S2.

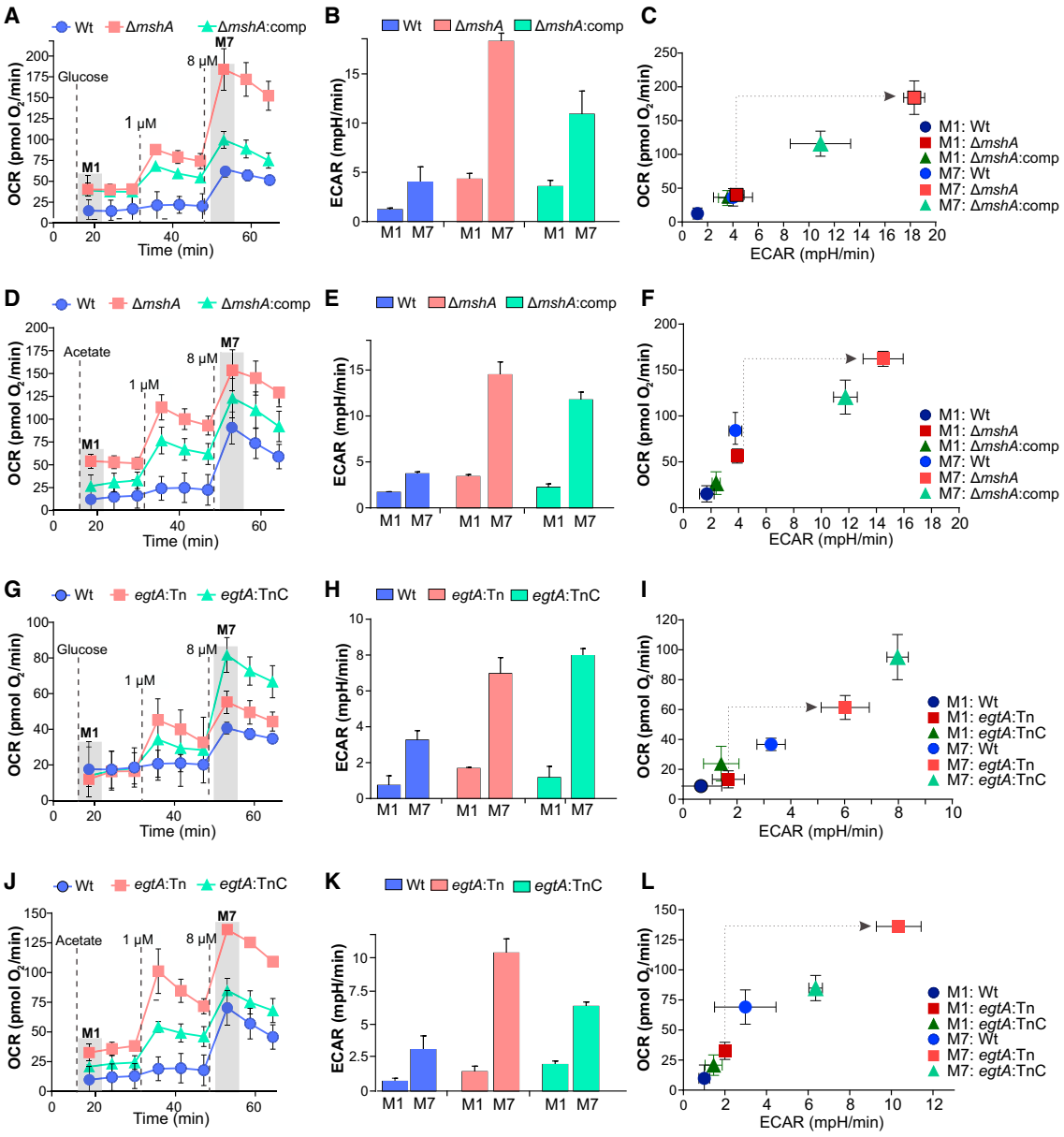

Figure 5. MSH and EGT Are Critical for Maintaining Bioenergetic Homeostasis in *Mtb*

(A–F) OCR profiles of WT *Mtb* (blue), Δ*mshA* (red), and Δ*mshA*:comp (green) (A and D). Also shown are corresponding ECAR measurements (B and E) and phenograms (C and F) of the three strains at M1 and M7, with 50 μM glucose (A–C) or 50 μM acetate (D–F) as carbon sources.

(G–L) OCR profiles of WT *Mtb* (blue), *egtA*:Tn (red), and *egtA*:TnC (green) (G and J); corresponding ECAR measurements (H and K). Phenograms (I and L) of the three strains are shown at M1 and M7, with 50 μM glucose (G–I) or 50 μM acetate (J–L) as a carbon source. Error bars represent SEM; n ≥ 16.

CCCP to a final concentration of 1 μM and 8 μM is indicated by vertical dotted lines in (A), (D), (G), and (J).

EGT and MSH Are Critical for Bioenergetic Homeostasis in *Mtb*

Since reduction/oxidation reactions (redox) and energy metabolism are intricately linked, we tested the hypothesis that redox buffers MSH and EGT are essential for maintaining bioenergetic homeostasis. Extracellular flux analysis showed alterations in the bioenergetic profiles (OCR and ECAR) of *mshA* and *egtA* mutant strains when using glucose or acetate as the sole carbon source. Genetic complementation of these mutants restored the bioenergetic phenotype comparable to WT, suggesting that lack of either EGT or MSH alters respiration in *Mtb* (Figures 5A–5L). The OCR (M1) of *egtA*:Tn and Δ*mshA* grown in acetate was higher than that of their respective WT strains (Figures 5D and 5J). However, addition of CCCP (M7) resulted in an increase in OCR (Figures 5A, 5D, and 5J) and ECAR (Figures 5B, 5E, and 5K) of *egtA* and *mshA* mutants that was significantly greater than that of WT and complemented strains, with the exception of the *egtA* complemented strain in glucose (M7, Figures 5G and 5H). This is also

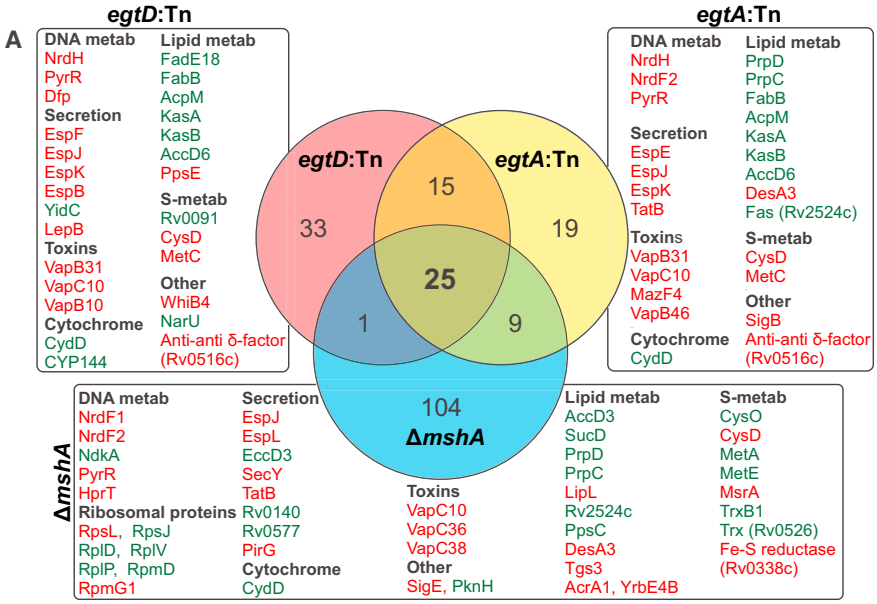

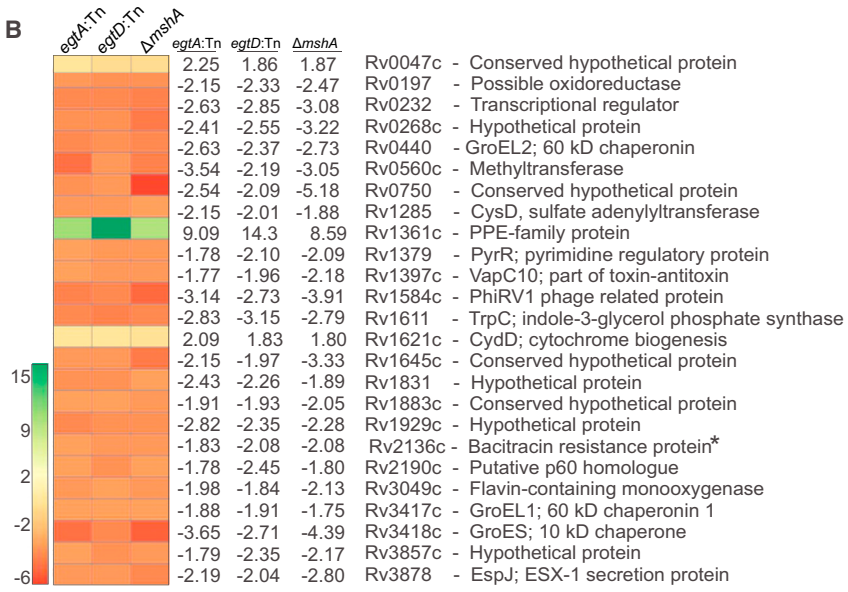

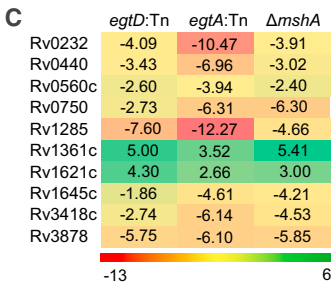

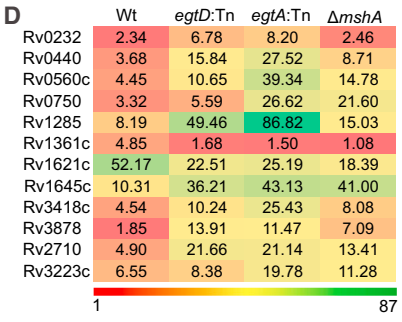

Figure 6. Whole-Genome Transcriptional Profiling of WT *Mtb*, *egtA*:Tn, *egtD*:Tn, and Δ*mshA*

(A) Illustration of the overlap of the transcriptomic response of *Mtb* mutants defective in EGT and MSH production (Venn diagram). Also shown are selected subsets of differentially regulated genes in each strain classified according to function. Green: up-regulation, red: downregulation. See Figures S4–S6 for a detailed list of differentially regulated genes.

(B) Microarray analysis of *egtA*:Tn, *egtD*:Tn, and Δ*mshA* grown under normal conditions identified a common set of 25 genes, 22 of which were downregulated. Genes displaying at least 1.75-fold variation in expression, with a q value of 1%, were considered to be differentially regulated. The q value is the equivalent of the p value after multiple-testing correction (see Supplemental Experimental Procedures).

(C) Quantitative real-time PCR analysis of a subset (10 of 25) of genes under normal growth conditions to validate microarray profiles. Expression of *sigA* was used as an internal control, and gene expression values were normalized to WT (Manganelli et al., 1999).

(D) Fold change in gene expression upon exposure to oxidative stress (CHP) relative to expression in unexposed cells. Expression of *sigB* (Rv2710) and *sigH* (Rv3223c) was used as a positive control to evaluate oxidative stress response.

*Sole gene (Rv2136c) unaffected by any uncoupler, respiratory inhibitor, membrane potential, or ΔpH modulator (Boshoff et al., 2004).

See also Figures S4–S6 and Tables S3 and S4.

highlighted in the phenograms in Figures 5C, 5F, 5I, and 5L, where clear shifts occur from low OCR and ECAR in the mutants at M1 to higher OCR and ECAR than the WT and complemented strains at M7. Importantly, the substantially different bioenergetic profiles upon addition of an uncoupler suggest electron transport chain dysfunction in the mutants resulting in greater OCR and ECAR in order to reestablish their membrane potentials. The unexpectedly high OCR observed in the *egtA* complemented strain at the higher concentration of CCCP (M7, Figure 5G) could be due to aberrant behavior of constitutive *hsp60* promoter in the episomal plasmid of the complement and has been observed previously in metabolic studies (Hartman et al., 2014). In sum, our data support the paradigm that alterations in redox status can modulate bioenergetic functions in *Mtb* cells.

Identification of Differentially Regulated Genes in EGT- and MSH-Deficient *Mtb*

Genes that contribute toward maintaining endogenous redox balance in *Mtb* are not well defined. To identify this core subset of genes, we carried out whole-genome transcriptomic profiling and compared the gene expression profiles of *Mtb* strains deficient in *egtA* (Figure S4), *egtD* (Figure S5), and *mshA* (Figure S6). Compared to WT *Mtb*, 139 genes are differentially expressed in

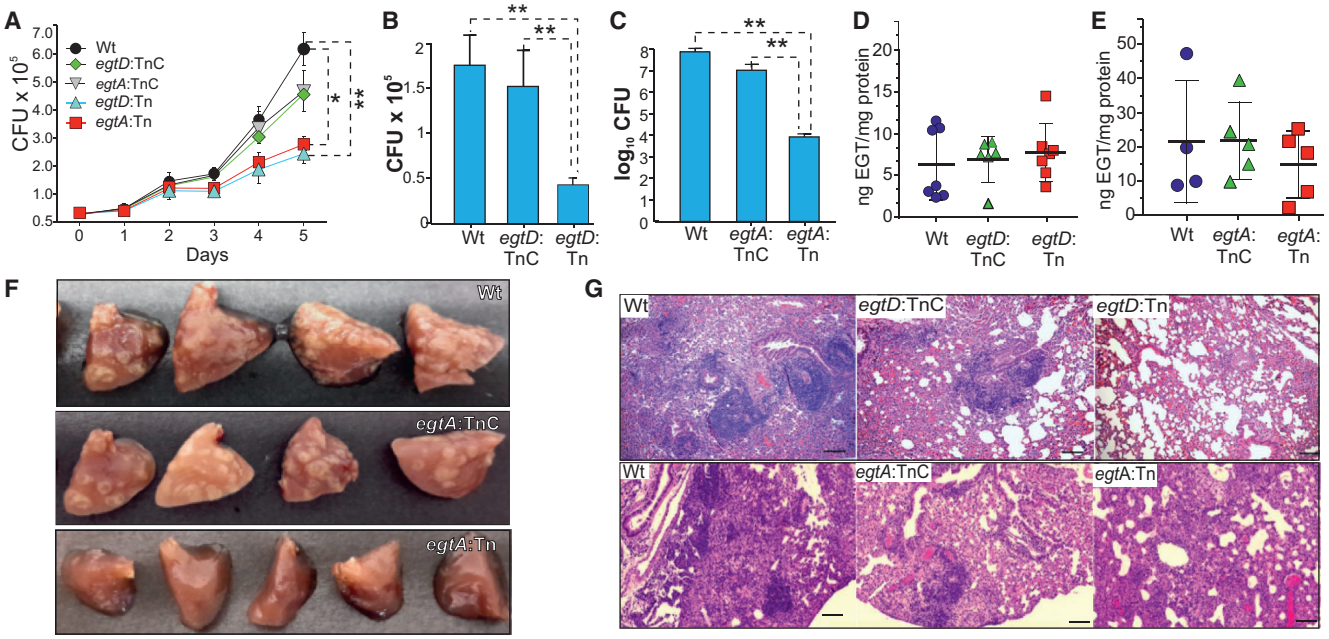

Figure 7. Survival and Pathogenicity of *Mtb egt* Mutants in Macrophages and Mice

(A) Survival of WT *Mtb*, *egtA*:Tn, *egtD*:Tn, and the corresponding complemented strains following macrophage infection. At the indicated time points, infected cells were lysed (n = 3) and lysates plated to enumerate CFUs. Each data point represents the mean ± SEM (*p = 0.0142, and **p = 0.0093).

(B–E) Mice were infected with WT *Mtb*, *egtA*:Tn, *egtD*:Tn, or the complemented strains. At 5 weeks postinfection, lungs were processed, and bacillary burden (B and C) was determined. Columns represent the mean, and error bars represent the SD of the mean of 4–7 mice per group (**p < 0.01). Corresponding EGT concentrations (D and E) were determined. Horizontal lines show the mean, and error bars represent the SD of the mean of 4–7 mice per group.

(F) Gross pathology of mouse lungs infected with WT *Mtb*, *egtA*:Tn, and *egtA*:TnC.

(G) H&E staining of lung tissue from infected mice (10× magnification). Scale bar, 100 μm.

Δ*mshA*, and 68 and 74 genes in the *egtA* and *egtD* mutant strains, respectively (Figure 6A). Notably, a common set of 25 genes was differentially regulated across all three strains (Figure 6B). The changes in gene expression observed in the microarray analysis were validated independently in *egtA*:Tn, *egtD*:Tn, and Δ*mshA* by quantitative real-time PCR analysis on a select subset of 10 genes (Figure 6C). Quantitative real-time PCR analysis of *egtA*:TnC, *egtD*:TnC, and Δ*mshA*:comp yielded gene expression values comparable to WT (Table S3).

Importantly, 24 of the 25 differentially regulated genes shared by the EGT- and MSH-deficient strains are differentially regulated by inhibitors of respiration (KCN, thioridazine, and 2,4-dinitrophenol), uncouplers (CCCP and N,N′-dicyclohexylcarbodiimide), or compounds that target an energized membrane (valinomycin) or ΔpH (nigericin) (Boshoff et al., 2004). Further, exposure of WT and all three mutant strains to oxidative stress (CHP) resulted in substantially increased expression of the same subset of 10 genes used in the microarray validation (Figure 6D). This observation underscores the importance of this core set of genes in redox regulation in *Mtb* in the absence of EGT and MSH under conditions of increased oxidative stress.

These data demonstrate that a lack of EGT or MSH results in differential expression of genes involved in nucleotide and sulfur metabolism, secretion, toxin/anti-toxins, lipid metabolism, and cytochrome biogenesis, likely as a compensatory response to the loss of redox couples. The regulation of *trx* genes by MSH, but not by EGT, is possibly an indicator of distinct chemical and functional requirements of mycobacterial redox buffers.

EGT Biosynthesis by *Mtb* Is Required for Survival in Macrophages and Mice

We next examined the role of EGT in intracellular *Mtb* survival and virulence. We observed significantly reduced survival of *egtA*:Tn and *egtD*:Tn in RAW264.7 macrophages at 5 days post-infection compared to WT *Mtb* (Figure 7A). Complementation of the *egtA*/*egtD* mutants restored intracellular survival to near WT levels. To determine the role of EGT in *Mtb* pathogenicity, mice were infected with WT, *egtD*:Tn, *egtA*:Tn, or the complemented strains in two independent experiments. We observed significantly reduced bacillary burdens in the lungs of mice infected with *egtD*:Tn or *egtA*:Tn compared to mice infected with WT *Mtb*. Complementation of *egtD*:Tn and *egtA*:Tn successfully restored bacillary load to WT levels. The *egtD*:Tn showed ~4-fold decrease in lung bacillary burden, whereas the *egtA*:Tn showed a 4-$\log_{10}$ reduction (Figures 7B and 7C). Multiple lesions were observed in the lungs of mice infected with WT and *egtA*:TnC strains compared to lungs of mice infected with *egtA*:Tn (Figure 7F). Histopathological analysis of lung sections from mice infected with WT *Mtb*, *egtA*:TnC, and *egtD*:TnC strains revealed large areas of alveolar consolidation due to lymphocyte-rich granulomatous infiltration (Figure 7G). In addition, multinucleated giant cells were observed in and around granulomas in the lungs of these mice. In contrast,

egtA:Tn- and *egtD*:Tn-infected lungs showed diffuse areas of lymphocyte infiltration and exhibited visible alveolar spaces with partial lung parenchyma.

Although it is known that EGT accumulates in organs that encounter oxidative stress (Cheah and Halliwell, 2012), it is not known whether infection by *Mtb* promotes accumulation of host-derived EGT or whether *Mtb* itself contributes significantly to the host EGT pool. Infection of macrophages with WT *Mtb*, *egtD*:Tn, *egtA*:Tn, and complemented strains (*egtD*:TnC and *egtA*:TnC) showed no significant difference in intracellular EGT concentrations (data not shown). Also, in mice infected with WT *Mtb*, *egtD*:Tn, *egtA*:Tn, or the complemented strains, we observed no statistically significant differences in lung EGT concentrations (Figures 7D and 7E). Altogether, our findings suggest that *Mtb* is not a significant contributor to host EGT during infection. In sum, independent disruption of two different genes within the EGT biosynthetic pathway results in attenuation in vivo and provides strong evidence for a role of EGT in *Mtb* intracellular survival and virulence.

DISCUSSION

The aim of this study was to examine how *Mtb* WhiB3 maintains intracellular redox homeostasis and bioenergetics to regulate virulence. Here, we discovered that the virulence factor WhiB3 is a regulator of bioenergetic homeostasis and controls the production of a major redox buffer EGT in a carbon-source-dependent manner to maintain redox balance. Furthermore, by successfully adapting extracellular flux analysis technology, we have shown that a lack of EGT or MSH significantly alters *Mtb* respiratory activity, which establishes a direct link between redox homeostasis and bioenergetic metabolism. Importantly, we provide evidence that redox and bioenergetic homeostasis contribute to *Mtb* survival in macrophages and in mice and are critical components in drug susceptibility and sensitivity to oxidative stress. The identification of bioenergetic deficiencies in *Mtb* mutants that display no apparent phenotypic defects when grown in vitro, but that demonstrate attenuation upon mouse infection, points to bioenergetic homeostasis as a largely overlooked but important factor in *Mtb* pathogenicity. We anticipate that bioenergetic homeostasis will broadly influence the study of microbial bioenergetics and pathogenesis. In sum, we have uncovered a dynamic balance between *Mtb* redox and bioenergetic homeostasis, which critically influences *Mtb* drug susceptibility and pathogenicity.

Our data indicate interdependency among central carbon metabolism, bioenergetic homeostasis, and redox balance in *Mtb* that ultimately affects drug susceptibility. This is in line with increasing evidence of the link between bacterial metabolism and drug susceptibility. For example, Lobritz et al. (2015) demonstrated a link between cellular respiration in *Escherichia coli* and *Staphylococcus aureus* and antibiotic efficacy. Peng et al. (2015) showed that promoting TCA flux to increase reduced nicotinamide adenine dinucleotide (NADH) and consequently proton motive force in multidrug-resistant *Edwardsiella tarda* restored susceptibility to kanamycin. In the case of *Mtb*, metabolic profiling revealed that exposure to sub-lethal concentrations of INH, RIF, and streptomycin remodeled *Mtb* central carbon metabolism to enable antibiotic tolerance (Nandakumar et al., 2014). In addition, growth-limiting stresses that redirect *Mtb* carbon flux away from central carbon metabolism toward triglyceride synthesis have been shown to diminish antibiotic sensitivity (Baek et al., 2011). Our data affirm this link between metabolism and antibiotic efficacy and show how the bioenergetic and redox status of *Mtb*, in which EGT and MSH play a role, affect drug susceptibility. Likewise, our study indicates that the roles of EGT and MSH in bioenergetic and redox homeostasis are essential for the resilience of *Mtb* against oxidative stress, which is necessary for full virulence of *Mtb*.

What is the biological significance of having two redox buffers, EGT and MSH, to protect *Mtb* against oxidative environments? One explanation rests in the inherent physicochemical properties of these redox intermediaries. For example, the reduction potential ($E^{0\prime}$) of EGT is −60 mV, and although the $E^{0\prime}$ of MSH has not been determined, it is speculated to be in the range of −200 to −320 mV, as is typical for other naturally occurring thiols (Hartman, 1990). This would enable EGT and MSH to respond differently to a spectrum of oxido-reductive stresses to facilitate a successful infection. This redox hierarchy may be critical to infection as EGT has been shown to function as a scavenger of singlet oxygen, $HO^{\bullet}$, $ONOO^{-}$, and HOCl radicals (Akanmu et al., 1991). Conversely, MSH has been shown to play a protective role against $^{\bullet}NO$ and CHP (alkyl peroxy radicals) (Miller et al., 2007). Notably, EGT does not readily undergo auto-oxidation and exists predominantly in the thione form rather than the thiol form, which confers greater stability compared to other thiols such as glutathione and MSH (Heath and Wildy, 1956). The reduction of MSSM to MSH requires an enzymatic system composed of a mycoredoxin, mycothiol disulfide reductase (Mtr) and reduced nicotinamide adenine dinucleotide phosphate (NADPH) (Patel and Blanchard, 1999), making this a highly complex system compared to EGT (Cheah and Halliwell, 2012). Altogether, these physicochemical differences likely explain the overlapping but distinct functions of EGT and MSH and the need for redundancy in redox buffers in this highly evolved pathogen.

This EGT/MSH redox hierarchy is also a critical parameter in drug susceptibility and therefore has strong clinical relevance. For example, we found that *egtA*/*egtD* and *mshA* mutants are more susceptible than WT *Mtb* to RIF, INH, CFZ, and the new anti-TB drug BDQ. The *egtA*/*egtD* mutants are less sensitive than the *mshA* mutant to BDQ and CFZ, both of which target the *Mtb* electron transport chain (Complex V and Complex I, respectively), thus implicating redox balance and bioenergetic homeostasis in modulating drug susceptibility. The dissimilarities in drug susceptibility phenotypes between EGT and MSH mutants may be due to the increased levels of EGT observed in the MSH mutant. MSH deficiency has been reported to lead to ethionamide resistance (Vilchèze et al., 2008) and rifampin sensitivity (Buchmeier et al., 2003). Altogether, our results highlight similar yet distinct roles for EGT and MSH in maintaining redox balance and conferring drug susceptibility through different redox or energy-mediated mechanisms.

The ability of EGT to protect against oxidative stress caused by CHP, PQT, H_2O_2, and MND confirms that *Mtb* produces EGT to maintain redox balance. Not all oxidative stresses are equal, as evidenced by differences in *Mtb* survival in the

presence of various oxidants and the fact that a broad spectrum of free radical reactions exists, ranging from very reducing (e.g., $E^{o'} = -1{,}800$ mV for $CO_2/CO_2^{\bullet-}$) to very oxidizing (e.g., $E^{o'} = 2{,}310$ mV for $HO^{\bullet}$, H^+/H_2O) (Buettner, 1993). The production of both EGT and MSH to counter free radicals may partially explain the remarkable success of *Mtb* as an intracellular pathogen that persists for decades in the oxidative environment of the lung. This work also establishes a relationship between EGT and MSH production. Notably, the increased EGT levels and reduced endogenous ROS (Figure 4F) in Δ*mshA* reveal the presence of a compensatory mechanism wherein EGT production is increased to mitigate endogenous oxidative stress in the absence of MSH. Collectively, the data support that the level of EGT in the cell, which is modulated by WhiB3 and the availability of carbon sources, serves as a buffer against redox stress such as $O_2^{\bullet-}$ associated with cellular metabolic activity. The implication of this finding is significant as carbon sources such as fatty acids or oxidation products can modulate redox balance and thus drug susceptibility during infection by varying EGT levels.

To understand the effects of EGT or MSH deficiency on global gene expression in *Mtb*, we performed transcriptomic analysis of *egtA*, *egtD*, and *mshA* mutants and identified 25 differentially regulated genes common to all three mutants. Our quantitative real-time PCR validation underscored the accuracy of our microarray-based gene expression analysis. Of these 25 genes, 24 are also modulated by respiration inhibitors, uncouplers, or compounds that target an energized membrane (Boshoff et al., 2004), implicating EGT and MSH in maintenance of bioenergetic homeostasis. Our observations elucidate a bioenergetics-centered model of WhiB3-mediated redox balance through EGT and represent a paradigm for redox homeostasis in prokaryotes.

Upregulation of an operon involved in mycolic acid biosynthesis (Rv2243–Rv2247) in the *egtA/egtD* mutants and of the Rv1130–Rv1131 operon (encoding PrpD and PrpC in the methylcitrate cycle) in the *mshA* and *egtA* mutants suggests that perturbations in redox balance due to lack of EGT or MSH affect biosynthesis of different classes of lipids, which may act as sinks for reducing equivalents (Singh et al., 2009). An important dissimilarity between the expression profiles of *egtA/egtD* and *mshA* mutants is that thioredoxin B (*trxB1*, Rv1471) and a putative thioredoxin-like gene (*trx*, Rv0526) are upregulated in the *mshA* mutant, but not in the *egtA/egtD* mutants. This observation is consistent with the requirement of MSH for thioredoxins as reducing partners (Attarian et al., 2009). The majority of the differentially regulated genes (22 of 25) in the *egtA/egtD* and *mshA* mutants are downregulated. Interestingly, 17 of the 22 downregulated genes are upregulated (2- to 5-fold) during *Mtb* infection of macrophages or under nutrient deprivation conditions in vitro (Schnappinger et al., 2003; Betts et al., 2002). It is therefore reasonable to posit that redox buffers EGT or MSH may also modulate the survival of *Mtb* inside macrophages and thus influence the outcome of infection.

Our in vitro and in vivo infection studies clearly show that EGT-deficient *Mtb* strains are attenuated and establish that EGT is critical for the intracellular survival and virulence of *Mtb* (Figures 7A–7C and 7F). These results provide important insights into the role of EGT in *Mtb* virulence in addition to its role in drug susceptibility, both of which appear to be distinct from MSH (Vilchèze et al., 2008). The observation that *egtA* and *egtD* contribute to different degrees to intracellular survival is supported by the finding that different intermediates of EGT biosynthesis may perform antioxidant functions (Song et al., 2015) and feed into different pathways of central carbon metabolism. Consequently, disruption of different steps in the EGT biosynthetic pathway in the *egtA* and *egtD* mutants likely explains the differences in attenuation (Figures 7A–7C, 7F, and 7G).

In summary, the findings in this study reveal new mechanisms by which *Mtb* perceives and relays metabolic signals to maintain redox balance and bioenergetic homeostasis. These findings establish important roles for EGT in oxidative stress protection, drug susceptibility, and virulence in *Mtb*, which are unlike MSH. The discovery of an EGT/MSH hierarchy of redox defense mechanisms with distinct physicochemical properties to counteract a spectrum of host-generated free radicals and metabolites has significant implications for how *Mtb* maintains redox and bioenergetic homeostasis during persistence.

EXPERIMENTAL PROCEDURES

Bacterial Strains and Culture Conditions

All *Mtb* strains used in this study, unless otherwise specified, were grown at 37°C in GIBCO Middlebrook (MB)7H9 (broth) or MB7H10/MB7H11 (agar) media supplemented with 0.2% glycerol, 1× ADST (albumin saline enrichment [albumin-NaCl] with 0.05% tyloxapol) as described in Supplemental Experimental Procedures.

Liquid Chromatography-Mass Spectrometry for Metabolome Analysis

Metabolites were separated on a Cogent Diamond Hydride Type C column and analyzed by LC-MS as described in Supplemental Experimental Procedures.

Bioenergetic Analysis of *Mtb*

OCR and ECAR of *Mtb* strains adhered to Cell-Tak-coated XF cell culture microplates (Seahorse Bioscience) at 2×10^6 bacilli/well were measured using an XF96 Extracellular Flux Analyzer as described in Supplemental Experimental Procedures.

TLC and LC-MS/MS Analysis of EGT

Cell extracts containing radiolabeled EGT were concentrated to dryness and resuspended in 50–100 μl of acetonitrile:methanol:50 mM ammonium acetate (40:40:20) (AMAA). At least 30,000 cpm in a maximum of 15 μl was loaded onto silica gel TLC plates and developed in a 3:1 methanol:water solvent system as described in Supplemental Experimental Procedures. To validate TLC analysis of EGT, concentrated, unlabeled *Msm* extract was loaded on a silica gel TLC plate and developed as above. The suspected EGT spot was visualized under UV light, scraped from the plate, and extracted four times with 50 μl AMAA. It was then concentrated to dryness, resuspended in 20 μl AMAA, and examined by an AB Sciex API-3200 Triple Quadrupole coupled to a Waters Acquity LC system. Data were collected in the positive electrospray mode. EGT levels in *Mtb* and mouse lungs were also determined using LC-MS/MS as described in Supplemental Experimental Procedures.

Measurement of Endogenous ROS in *Mtb*

The percentage of ROS-producing *Mtb* cells was determined using CellROX Green (Life Technologies) and flow cytometry as described in Supplemental Experimental Procedures.

Determination of *Mtb* Susceptibility to Oxidants and Anti-TB Drugs

Mtb cells were cultured as described above. *Mtb* strains were exposed to oxidizing agents (6 hr) or various concentrations of anti-TB drugs (7 days).

Cells were plated on MB7H11 agar plates, colonies were enumerated after 4 to 5 weeks of incubation at 37°C, and percentage survival was determined. Additional details are provided in Supplemental Experimental Procedures.

Microarray Analysis

Mtb RNA was isolated and prepared as described in Supplemental Experimental Procedures.

Quantitative Real-Time PCR Analysis

Total RNA was isolated from mycobacterial cells and quantitative real-time PCR analysis was performed as described in Supplemental Experimental Procedures.

Mtb Infection Studies and Quantitation of EGT

For in vitro infection studies, RAW264.7 macrophages were infected with *Mtb* strains at a MOI of ten. Mice were used as our in vivo model of infection. Experimental details are outlined in Supplemental Experimental Procedures.

Statistics

Statistical computations were performed with Prism 6.0 software (GraphPad). Pairwise comparison was performed by Student's t test for normally distributed data. Multiple comparisons were performed using one-way ANOVA (Tukey's test) module of GraphPad.

ACCESSION NUMBERS

The accession number for the microarray data reported in this paper is EMBL ArrayExpress: E-MTAB-4099.

SUPPLEMENTAL INFORMATION

Supplemental Information includes Supplemental Experimental Procedures, six figures, and four tables and can be found with this article online at http://dx.doi.org/10.1016/j.celrep.2015.12.056.

AUTHOR CONTRIBUTIONS

Conceptualization, V.S., L.G., and A.J.C.S.; Investigation, mass spectrometric and metabolomic analyses (J.H.A., H.E., and K.R.), quantitation of EGT and MSH (L.G., Y.A.-G., and H.B.), XF assays (D.L.), ROS determination (B.M.C.), transcriptomic profiling and analysis (V.S.), macrophage assays (K.C.C.), drug and oxidative stress susceptibility assays (V.S. and V.P.R.), animal studies at UAB (V.S., V.P.R., K.C.C., and J.N.G.) and KRITH (J.M. and M.R.-G.), and histopathological analysis (V.S. and V.P.R.); Validation, V.S. and K.C.C.; Data Curation, V.S., D.L., and K.R.; Writing, V.S., B.M.C., L.G., J.N.G., and A.J.C.S.; Funding Acquisition, A.J.C.S. All authors discussed the results and commented on the manuscript.

ACKNOWLEDGMENTS

This work was supported by NIH grants AI076389, AI058131, DOD Discovery Award PR121320, and pilot funds from the UAB Centers for AIDS Research and Free Radical Biology and UAB School of Medicine Infectious Diseases and Global Health and Vaccines Initiative to A.J.C.S. A.J.C.S. and K.R. are Burroughs Welcome Investigators in the Pathogenesis of Infectious Disease. V.S. was supported by Senior Research Training Fellowship RT-232840-N from the American Lung Association. The research from which this publication emanated was co-funded by the South African Medical Research Council. The authors thank Amit Singh for helpful discussions, Nicholas J. Eustace for technical assistance, William R. Jacobs Jr. (Albert Einstein College of Medicine) for providing Δ*mshA*, and Digby Warner (University of Cape Town) for providing bedaquiline. Open access publication of this article has been made possible through support from the Victor Daitz Information Gateway, an initiative of the Victor Daitz Foundation and the University of KwaZulu-Natal.

Received: August 22, 2015
Revised: October 30, 2015
Accepted: December 9, 2015
Published: January 7, 2016

REFERENCES

Akanmu, D., Cecchini, R., Aruoma, O.I., and Halliwell, B. (1991). The antioxidant action of ergothioneine. Arch. Biochem. Biophys. *288*, 10–16.

Attarian, R., Bennie, C., Bach, H., and Av-Gay, Y. (2009). Glutathione disulfide and S-nitrosoglutathione detoxification by *Mycobacterium tuberculosis* thioredoxin system. FEBS Lett. *583*, 3215–3220.

Baek, S.H., Li, A.H., and Sassetti, C.M. (2011). Metabolic regulation of mycobacterial growth and antibiotic sensitivity. PLoS Biol. *9*, e1001065.

Betts, J.C., Lukey, P.T., Robb, L.C., McAdam, R.A., and Duncan, K. (2002). Evaluation of a nutrient starvation model of *Mycobacterium tuberculosis* persistence by gene and protein expression profiling. Mol. Microbiol. *43*, 717–731.

Boshoff, H.I., Myers, T.G., Copp, B.R., McNeil, M.R., Wilson, M.A., and Barry, C.E., 3rd. (2004). The transcriptional responses of *Mycobacterium tuberculosis* to inhibitors of metabolism: novel insights into drug mechanisms of action. J. Biol. Chem. *279*, 40174–40184.

Buchmeier, N.A., Newton, G.L., Koledin, T., and Fahey, R.C. (2003). Association of mycothiol with protection of *Mycobacterium tuberculosis* from toxic oxidants and antibiotics. Mol. Microbiol. *47*, 1723–1732.

Buettner, G.R. (1993). The pecking order of free radicals and antioxidants: lipid peroxidation, alpha-tocopherol, and ascorbate. Arch. Biochem. Biophys. *300*, 535–543.

Cheah, I.K., and Halliwell, B. (2012). Ergothioneine; antioxidant potential, physiological function and role in disease. Biochim. Biophys. Acta *1822*, 784–793.

de Carvalho, L.P., Fischer, S.M., Marrero, J., Nathan, C., Ehrt, S., and Rhee, K.Y. (2010). Metabolomics of *Mycobacterium tuberculosis* reveals compartmentalized co-catabolism of carbon substrates. Chem. Biol. *17*, 1122–1131.

Everts, B., Amiel, E., Huang, S.C., Smith, A.M., Chang, C.H., Lam, W.Y., Redmann, V., Freitas, T.C., Blagih, J., van der Windt, G.J., et al. (2014). TLR-driven early glycolytic reprogramming via the kinases TBK1-IKKε supports the anabolic demands of dendritic cell activation. Nat. Immunol. *15*, 323–332.

Ferrick, D.A., Neilson, A., and Beeson, C. (2008). Advances in measuring cellular bioenergetics using extracellular flux. Drug Discov. Today *13*, 268–274.

Genghof, D.S. (1970). Biosynthesis of ergothioneine and hercynine by fungi and Actinomycetales. J. Bacteriol. *103*, 475–478.

Hand, C.E., and Honek, J.F. (2005). Biological chemistry of naturally occurring thiols of microbial and marine origin. J. Nat. Prod. *68*, 293–308.

Hartman, P.E. (1990). Ergothioneine as antioxidant. Methods Enzymol. *186*, 310–318.

Hartman, T., Weinrick, B., Vilchèze, C., Berney, M., Tufariello, J., Cook, G.M., and Jacobs, W.R., Jr. (2014). Succinate dehydrogenase is the regulator of respiration in *Mycobacterium tuberculosis*. PLoS Pathog. *10*, e1004510.

Heath, H., and Wildy, J. (1956). The biosynthesis of ergothioneine and histidine by *Claviceps purpurea*. I. The incorporation of [2-^{14}C]-acetate. Biochem. J. *64*, 612–620.

Kumar, A., Farhana, A., Guidry, L., Saini, V., Hondalus, M., and Steyn, A.J. (2011). Redox homeostasis in mycobacteria: the key to tuberculosis control? Expert Rev. Mol. Med. *13*, e39.

Lee, W., VanderVen, B.C., Fahey, R.J., and Russell, D.G. (2013). Intracellular *Mycobacterium tuberculosis* exploits host-derived fatty acids to limit metabolic stress. J. Biol. Chem. *288*, 6788–6800.

Lei, B., Wei, C.-J., and Tu, S.-C. (2000). Action mechanism of antitubercular isoniazid. Activation by *Mycobacterium tuberculosis* KatG, isolation, and characterization of inha inhibitor. J. Biol. Chem. *275*, 2520–2526.

Lobritz, M.A., Belenky, P., Porter, C.B., Gutierrez, A., Yang, J.H., Schwarz, E.G., Dwyer, D.J., Khalil, A.S., and Collins, J.J. (2015). Antibiotic efficacy is

linked to bacterial cellular respiration. Proc. Natl. Acad. Sci. USA *112*, 8173–8180.

Manganelli, R., Dubnau, E., Tyagi, S., Kramer, F.R., and Smith, I. (1999). Differential expression of 10 sigma factor genes in *Mycobacterium tuberculosis*. Mol. Microbiol. *31*, 715–724.

Miller, C.C., Rawat, M., Johnson, T., and Av-Gay, Y. (2007). Innate protection of *Mycobacterium smegmatis* against the antimicrobial activity of nitric oxide is provided by mycothiol. Antimicrob. Agents Chemother. *51*, 3364–3366.

Nandakumar, M., Nathan, C., and Rhee, K.Y. (2014). Isocitrate lyase mediates broad antibiotic tolerance in *Mycobacterium tuberculosis*. Nat. Commun. *5*, 4306.

Patel, M.P., and Blanchard, J.S. (1999). Expression, purification, and characterization of *Mycobacterium tuberculosis* mycothione reductase. Biochemistry *38*, 11827–11833.

Peng, B., Su, Y.B., Li, H., Han, Y., Guo, C., Tian, Y.M., and Peng, X.X. (2015). Exogenous alanine and/or glucose plus kanamycin kills antibiotic-resistant bacteria. Cell Metab. *21*, 249–261.

Rawat, M., Johnson, C., Cadiz, V., and Av-Gay, Y. (2007). Comparative analysis of mutants in the mycothiol biosynthesis pathway in *Mycobacterium smegmatis*. Biochem. Biophys. Res. Commun. *363*, 71–76.

Rhee, K.Y., de Carvalho, L.P., Bryk, R., Ehrt, S., Marrero, J., Park, S.W., Schnappinger, D., Venugopal, A., and Nathan, C. (2011). Central carbon metabolism in *Mycobacterium tuberculosis*: an unexpected frontier. Trends Microbiol. *19*, 307–314.

Richard-Greenblatt, M., Bach, H., Adamson, J., Peña-Diaz, S., Li, W., Steyn, A.J., and Av-Gay, Y. (2015). Regulation of Ergothioneine Biosynthesis and Its Effect on *Mycobacterium tuberculosis* Growth and Infectivity. J. Biol. Chem. *290*, 23064–23076.

Sao Emani, C., Williams, M.J., Wiid, I.J., Hiten, N.F., Viljoen, A.J., Pietersen, R.D., van Helden, P.D., and Baker, B. (2013). Ergothioneine is a secreted antioxidant in *Mycobacterium smegmatis*. Antimicrob. Agents Chemother. *57*, 3202–3207.

Schnappinger, D., Ehrt, S., Voskuil, M.I., Liu, Y., Mangan, J.A., Monahan, I.M., Dolganov, G., Efron, B., Butcher, P.D., Nathan, C., and Schoolnik, G.K. (2003). Transcriptional Adaptation of *Mycobacterium tuberculosis* within Macrophages: Insights into the Phagosomal Environment. J. Exp. Med. *198*, 693–704.

Seebeck, F.P. (2010). *In vitro* reconstitution of Mycobacterial ergothioneine biosynthesis. J. Am. Chem. Soc. *132*, 6632–6633.

Singh, A., Guidry, L., Narasimhulu, K.V., Mai, D., Trombley, J., Redding, K.E., Giles, G.I., Lancaster, J.R., Jr., and Steyn, A.J.C. (2007). *Mycobacterium tuberculosis* WhiB3 responds to O_2 and nitric oxide via its [4Fe-4S] cluster and is essential for nutrient starvation survival. Proc. Natl. Acad. Sci. USA *104*, 11562–11567.

Singh, A., Crossman, D.K., Mai, D., Guidry, L., Voskuil, M.I., Renfrow, M.B., and Steyn, A.J. (2009). *Mycobacterium tuberculosis* WhiB3 maintains redox homeostasis by regulating virulence lipid anabolism to modulate macrophage response. PLoS Pathog. *5*, e1000545.

Song, H., Hu, W., Naowarojna, N., Her, A.S., Wang, S., Desai, R., Qin, L., Chen, X., and Liu, P. (2015). Mechanistic studies of a novel C-S lyase in ergothioneine biosynthesis: the involvement of a sulfenic acid intermediate. Sci. Rep. *5*, 11870.

Steyn, A.J.C., Collins, D.M., Hondalus, M.K., Jacobs, W.R., Jr., Kawakami, R.P., and Bloom, B.R. (2002). *Mycobacterium tuberculosis* WhiB3 interacts with RpoV to affect host survival but is dispensable for in vivo growth. Proc. Natl. Acad. Sci. USA *99*, 3147–3152.

Vilchèze, C., Av-Gay, Y., Attarian, R., Liu, Z., Hazbón, M.H., Colangeli, R., Chen, B., Liu, W., Alland, D., Sacchettini, J.C., and Jacobs, W.R., Jr. (2008). Mycothiol biosynthesis is essential for ethionamide susceptibility in *Mycobacterium tuberculosis*. Mol. Microbiol. *69*, 1316–1329.